NJC

PAPER

View Article Online
View Journal | View Issue

Cite this: *New J. Chem.*, 2015, 39, 5203

Poly(vinylpyrrolidone) stabilized aluminum nanoparticles obtained by the reaction of $SiCl_4$ with $LiAlH_4$†

Sanyasinaidu Gottapu,[a] Santanu Kumar Padhi,[b] Mamidipudi Ghanashyam Krishna[b] and Krishnamurthi Muralidharan*[a]

Received (in Montpellier, France) 20th February 2015,
Accepted 21st April 2015

DOI: 10.1039/c5nj00438a

www.rsc.org/njc

Isolation and stabilization of Al nanoparticles has been possible by the room temperature reaction between $SiCl_4$ and $LiAlH_4$ in the presence of poly(vinylpyrrolidone) (PVP) under sonication. The present investigation explained that the Al from $LiAlH_4$ produced Al nanoparticles while $SiCl_4$ was converted to hydrosilanes. The formation of Al nanoparticles from this reaction was established by thorough characterization using PXRD patterns, ^{27}Al MAS-NMR spectra and HRTEM micrographs. The isolation of Al nanoparticles from this reaction clearly explained the products formed in this reaction.

1. Introduction

Silanes of types SiH_4 and $HSiCl_3$ are used in the organic synthesis, hydrosilation reactions, and in the syntheses of silicon nanoparticles and hypervalent silicon compounds.[1–4] The generation of pyrophoric hydrosilanes by the reduction of $SiCl_4$ using $LiAlH_4$ and the hazards associated with this reaction were well documented.[5] The reduction of respective tetrachlorides by $LiAlH_4$ yielding SiH_4, GeH_4 and SnH_4 was reported more than five decades ago.[6] $LiAlH_4$ was also used to produce GaH_3, BeH_2 and ZnH_2.[6] Curiously, few reports claimed the formation of silicon nanoparticles by the reduction of $SiCl_4$ using $LiAlH_4$.[7] However, none of the reports documented the fate of Al in $LiAlH_4$ after the reaction.

It was reported that when $AlCl_3$ was reduced by $LiAlH_4$, the Al from both the compounds yielded Al nanoparticles.[8,9] This reaction was believed to occur *via* the formation of a hydride dimer which subsequently decomposed yielding Al nanoparticles. Similarly, while exploring the reduction of $ZnCl_2$ using $LiBH_4$, we observed the evolution of BH_3 gas along with the Zn nanoparticles.[10] This reaction also yielded a trace amount of $[B_{12}H_{12}]^{2-}$. Though both these reactions explained the fate of Al and B in the reductants, it has not been mentioned in many reactions. In this scenario, we have now concluded that Al nanoparticles[8,9] were essentially the main products along with hydrosilanes in the reaction of $SiCl_4$ with $LiAlH_4$.

2. Experimental section

2.1 Materials

Lithium aluminium hydride, $SiCl_4$, and poly(vinylpyrrolidone) (PVP) (Mol. wt. 10 000) were purchased from Sigma-Aldrich and used without further purification. Toluene was refluxed with sodium and benzophenone followed by distillation under a nitrogen atmosphere and was stored on 4 Å molecular sieves. The solvent was degassed by freeze–pump–thaw cycles for 3 times prior to the use. Methanol dried with magnesium methoxide was used for the quenching of excess $LiAlH_4$ and extraction of reaction by-product(s).

2.2 Synthesis of aluminium nanoparticles

The synthesis was carried out using the Schlenk technique in a N_2 atmosphere. In a 50 mL two neck round bottom flask with a N_2 gas inlet and outlet, $LiAlH_4$ (0.165 g, 4.36 mmol) was suspended in degassed toluene (15 mL) and then $SiCl_4$ (0.5 mL, 4.36 mmol) was added in drops. The reaction vessel was kept in an ultrasonic water bath with continuous sonication for 1 h under the stream of nitrogen. It was observed that the bulk solution temperature reached 56 °C which was sufficient enough to remove the low boiling silanes and other gaseous by-products formed in this reaction. However, the formation of silane(s) in this reaction was identified from the ^{29}Si NMR spectrum (Fig. S1, ESI†) of the reaction mixture which was cooled to ice temperature. The reaction mixture was quenched by excess MeOH under cold

[a] *School of Chemistry, University of Hyderabad, Gachibowli, Hyderabad, Telangana, India-500046. E-mail: kmsc@uohyd.erent.in*
[b] *School of Physics and Advanced Centre of Research in High Energy Materials (ACRHEM), University of Hyderabad, Gachibowli, Hyderabad, Telangana, India-500046*

† Electronic supplementary information (ESI) available: Additional information on solid state MAS-NMR, the selected area electron diffraction pattern of Al-nanocrystals, PXRD and TEM images. See DOI: 10.1039/c5nj00438a

$$SiCl_4 + LiAlH_4 \xrightarrow[1h,\ sonication]{Toluene} Al + H_2\uparrow + LiCl + (H)_x(SiCl)_{4-x}\uparrow$$

Scheme 1 Synthesis of aluminium nanoparticles.

conditions to avoid thermal runway and then Al nanoparticles were extracted by filtration. The product was again washed with dry methanol to obtain pure product in 68.1% yield which was characterized by a PXRD pattern (Fig. S2, ESI†) and TEM images (Fig. S3, ESI†). The plausible stoichimetry of this reaction is shown in Scheme 1.

2.3 Synthesis of Al–polymer nanocomposite

In another reaction, $LiAlH_4$ (0.165 g, 4.36 mmol) was suspended in degassed toluene (15 mL) along with 0.058 g of poly-(vinylpyrrolidone) and then $SiCl_4$ (0.5 mL, 4.36 mmol) was added in drops. The reaction was continued similar to the above procedure but with an extended time (2 h). The weight of the polymer added was the weight required to obtain a 2 : 1 theoretical weight ratio of metal to polymer composite assuming a 100% yield of aluminium (0.117 g, 4.36 mmol) in the reaction. The reaction mixture was quenched by adding excess MeOH under cold conditions and filtered to yield Al nanoparticles embedded in the PVP matrix (Scheme 2). The grey Al–PVP nanocomposite powder was washed with dried methanol to remove impurities and then characterized by PXRD patterns (Fig. 1).

2.4 Instrumentation

Powder X-ray diffraction (PXRD) was carried out using a Bruker D8 X-ray diffractometer [λ (Cu-Kα) = 1.54 Å]. The spectrum was recorded with 2θ ranging from 10° to 85° with a scan rate of 1° min^{-1}. The isotropic solid state ^{27}Al (100% abundant, $I = 1/2$) NMR spectra were recorded with 4 kHz MAS speed with the following acquisition parameters using a Brucker Advance 400 spectrometer (^{27}Al resonance frequency of 104.34 MHz): FID was recorded at a 4 K data point with a scanning width of 312 kHz. The number of accumulations was 512 with a pulse width of 3.9 μs and 0.5 s recycle delay. For each analysis, about 100 mg of the Al–PVP composite powder was filled in the zirconia rotor under a nitrogen atmosphere and caped with KEL-F caps. The Fourier transform infrared (FT-IR) spectra (KBr pellet) were recorded on a Jasco 5300 spectrophotometer.

A transmission electron microscope (TEM) FEI Tecnai 200 kV D2083 super twin in dark-field (DF), bright-field (BF) and high resolution (HR-TEM) mode was used for the analysis of nanoparticles and nanocomposites. The TEM samples were prepared by suspending particles in MeOH followed by ultrasonication for 5 minutes. The carbon coated copper grid was dipped gently and then withdrawn horizontally. The grid was dried on a filter paper. TEM-EDX spectra were collected in conventional TEM mode by condensing the electron beam (typically 50–100 nm in diameter) to the region of interest. The Apollo XLT Silicon Drift detector was used for this purpose. Thermo gravimetric analysis (TG-DTA) was carried out on a TA instrument (SDT Q600), using an alumina crucible under flow of UHP nitrogen or argon gas (flow rate = 100 cm^3 min^{-1}) as protective gas. The samples (~1 mg) were analysed from room temperature to 1300 °C at a heating rate of 50 °C min^{-1}.

$$SiCl_4 + LiAlH_4 \xrightarrow[2h,\ sonication]{Toluene,\ PVP} Al\text{-}NPs/PVP + H_2\uparrow + LiCl + (H)_xSi(Cl)_{4-x}\uparrow$$

Scheme 2 Synthesis of Al–polymer nanocomposites.

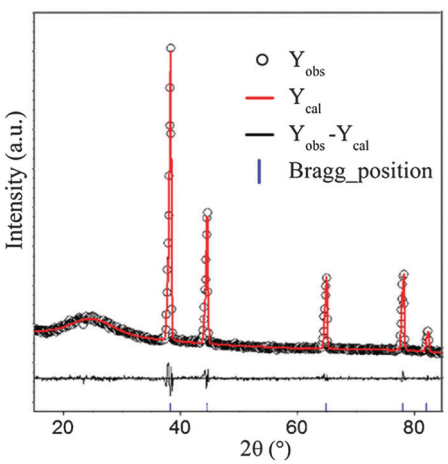

Fig. 1 Rietveld refined PXRD pattern of synthesized Al–PVP composites.

3. Results and discussion

3.1 Synthesis and characterization of Al nanoparticles

In our continuous effort to develop synthetic methodologies[9–11] for the metal and metal sulphide nanoparticles, we have investigated the reaction of $SiCl_4$ with $LiAlH_4$ with emphasis on understanding the fate of Al in the reaction.[5–7] Interestingly, the reaction of $LiAlH_4$ with $SiCl_4$ in toluene on exposure to ultrasound (sonication) yielded Al nanoparticles as the main product along with hydrosilanes (H_xSiCl_{4-x}).

The PXRD pattern (Fig. S2, ESI†) of the isolated solid confirmed the formation of Al, while its purity was confirmed by the solid state ^{27}Al MAS NMR spectrum. The TEM images of freshly prepared Al (Fig. S3, ESI†) clearly showed crystalline nanoparticles. The HRTEM images (Fig. S4, ESI†) of uncoated Al particles indicated that surfaces were composed of lattice fringes of about 2.32 Å, representing (111) crystal planes of FCC Al. Corresponding SAED (Fig. S4b, ESI†) confirmed the single crystalline nature of bare Al particles. Uncoated Al particles were sensitive to atmosphere and get oxidized upon exposure to air.

The formation of Al was further established by thorough characterization of polymer coated Al nanoparticles that were produced using this reaction (*vide infra*). The formation of hydrosilanes in this reaction was well documented in the literature.[5,6] We have confirmed the formation of hydorsilanes in our reaction using a complicated ^{29}Si NMR spectrum (Fig. S1, ESI†) of the reaction mixture. The isolation of any silanes from

our reaction was unsuccessful owing to the miniscule quantity and volatility.

A large number of reactions in both organic and inorganic chemistry are known wherein $LiAlH_4$ was used as the reducing agent. The mechanism of this reduction/hydrogenation was well established in organic synthesis.[12] However, the product from the reaction involving $LiAlH_4$ in inorganic synthesis was dictated by various factors including the nature of the substrate.[5–7] For example, the reaction between $LiAlH_4$ and $AlCl_3$ yielded Al nanoparticles *via* an aluminium hydride intermediate.[8,9] Similarly, the formation of hydrosilanes from the reaction of $SiCl_4$ with $LiAlH_4$ was well established[5,6] while other reports claimed the formation of Si nanoparticles[7] from the same reaction. Those reports were contradicting with each other on the fate of Si, and also did not explain the fate of Al. In this scenario, we have proved the formation of phase pure Al nanoparticles by this reaction, while Si was left as hydrosilanes.

The mechanism of formation of products in this reaction can be explained as follows. In the first step, $LiAlH_4$ reduced $SiCl_4$ yielding silanes, LiCl and AlH_3. The formation of alane (AlH_3) from $LiAlH_3$ in reactions with $AlCl_3$ and other metal chlorides is well documented.[13] It is well known[14] that AlH_3 can be decomposed to yield Al and H_2 at the temperature range of 60–200 °C. Similarly, the alane formed in this reaction subsequently decomposed to form Al nanoparticles under sonication (Fig. S6, ESI†).

3.2 Al–PVP composite

There has been growing interest in the production of surface coated Al nanoparticles for use as fuel.[15,16] Therefore, the room temperature sonochemical synthesis described above was used for the production of poly(vinylpyrrolidone) (PVP) coated Al nanoparticles for potential use in thermite reactions. For this purpose, $SiCl_4$ was reacted with $LiAlH_4$ in the presence of PVP. The weight of the polymer, to obtain an Al : polymer weight ratio of 2 : 1, was decided assuming 100% theoretical yield of Al as per the stoichiometry of the reaction.

The solid state ^{27}Al MAS NMR spectrum showed a strong signal at 1639.4 ppm for Al–PVP nanoparticles (Fig. S7, ESI†). The absence of any signal corresponding to the hexa- (10–15 ppm), penta- (25–35 ppm) or tetra-coordinated (65–85 ppm) oxygen environment and AlN_4 (100–115 ppm) revealed the purity of embedded Al nanoparticles in the PVP matrix.[17] The X-ray powder diffractogram of the Al–polymer nanocomposite (Fig. 1) was matching well with JCPDS no. 89-4037 of crystalline Al and no aluminium oxide peaks were observed. The broad peak at a low angle region (2θ = 20°–30°) was mainly observed because of the amorphous nature of the PVP matrix.[18] The combination of Rietveld structural refinement of the crystalline phase and a single Split Pseudo-Voigt (SPV) peak fitting to the large amorphous bump was carried out using Brucker AXS TOPAS version 5. The refined Al lattice parameter (a) = 4.062 (003) Å and the quantity of the crystalline phase computed was 65.18(02)%. The outcome of the refinement shown in Fig. 1 had well enough standard R-factor (%) values, R_{exp} = 3.85, R_{wp} = 5.47 and goodness of fit index, χ^2 = 1.42.[19]

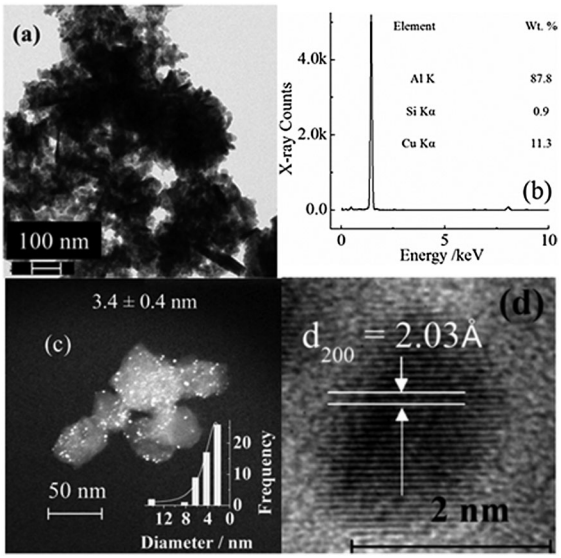

Fig. 2 Microstructural characterization of Al–PVP using TEM. (a) Low magnification image of Al–PVP grains in bright field mode, (b) EDX spectrum of Al–PVP showing elements wt%, (c) embedded Al nanoparticles (brighter spots) in the PVP matrix imaged in TEM dark field mode, and (d) high-magnification bright-field TEM showing Al d_{200} lattice fringes.

The Al–polymer composite was investigated in TEM to understand the morphology, composition and crystal structure of embedded Al nanoparticles. The TEM bright field (BF) image (Fig. 2a) revealed the agglomerated Al–PVP nanocomposite grains. Further observation of the same region in the dark-field (DF) mode with higher magnification revealed the embedded Al nanocrystals (brighter spots in Fig. 2c) as the source of selected area diffraction (SAED, Fig. S8, ESI†), but not the polymer matrix. Based on the TEM DF micrograph (Fig. 2c), it was realized that the current Al nanoparticle synthesis yielded fairly narrow spherical nanocrystals (2–15 nm) well embedded at random locations inside the PVP matrix. However, the mean size of particles of the Al–PVP composite calculated using the Williamson–Hall plot was 15.4 nm (Fig. S9, ESI†). The crystal lattice fringes of individual Al nanoparticles embedded in the PVP matrix were observed (Fig. 2d) in high resolution TEM (HR-TEM) mode. It indicated the monocrystalline nature of Al nanoparticles, consistent with the DF mode and the X-ray diffraction results presented above. The nanocrystal surfaces were covered with (200) planes of Al having 2.03 Å lattice spacing. The energy dispersive X-ray (EDX) analysis of the specimen confirmed the presence of 87.8 and 11.3 wt% of aluminium and copper (a part of the TEM grid) respectively and a relatively small 0.9 wt% of the Si residue from the precursor used.

The stabilization of Al nanoparticles in the PVP matrix was investigated using FT-IR spectroscopy (Fig. 3). The general observation was that PVP would coordinate with metal atoms through a polyvinyl skeleton, C–N and C═O polar groups. In the vibrational absorption spectrum of pure PVP, the wave numbers 1665 and 1070 cm^{-1} were assigned to the C═O and C–N bond. In our Al–PVP composite, the peak at 1665 cm^{-1} was

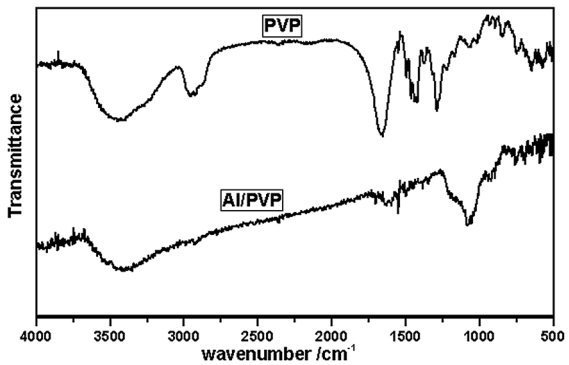

Fig. 3 FT-IR spectrum of PVP and Al–PVP nanocomposites.

shifted to 1620 cm^{-1} and C–N bond vibrations at 1070 cm^{-1} in PVP shifted to 923 cm^{-1} as a result of bond weakening. This can be attributed to partial donation of the lone pair of electrons forming a weak coordinative chemical bonding at the interfaces of Al and polymer. Thus the lone-pair of electrons of oxygen and nitrogen atoms in PVP involved coordinate bonding with atoms on the surface of aluminium nanoparticles. Also this surface coordination with PVP hindered the particle agglomeration and restricted the movement of embedded nanoparticles.

3.3 Thermal characterization

The temperature region of oxidation of Al nanoparticles embedded in the PVP matrix was examined by thermogravimetric (TGA) analysis. The thermogram at a heating rate of 50 °C min^{-1} (Fig. 4) depicted 23.02% weight loss up to 510 °C associated with PVP decomposition which would leave Al exposed for oxidation. Consequently, after the removal of the polymer by decomposition, a 56.03% gain in weight (from 76.98% to 133.01%) was observed up to 1275 °C which can be attributed to oxidation. From this weight gain the active Al content calculated from the TG curve following the procedure reported previously[20] was 63.03% (ESI†). The unaccounted 13.92% mass was due to (i) the formation of amorphous alumina (undetectable quantity in PXRD) in the synthesis, (ii) left out carbonaceous mass from burnt PVP in TG analysis and (iii) inherent error in active Al calculation because the TG temperature range of analysis did not reach the saturation point of Al oxidation.[21]

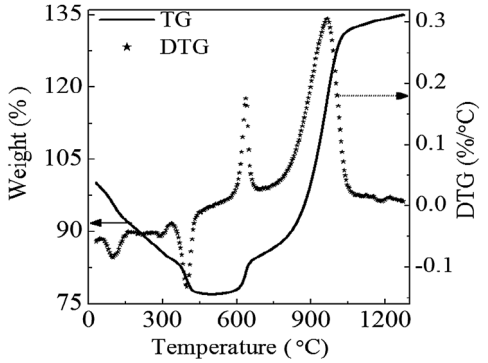

Fig. 4 TG-DTG curve revealing the regions of PVP decomposition and major amount of Al oxidation regions.

The entire Al oxidation region above 510 °C showed two distinct derivative thermogravimetry (DTG) peaks at 636.5 °C and 968 °C with 8.2% and 47.83% weight gains respectively. A similar two-step oxidation was reported previously.[22] The PXRD pattern of the residue obtained after TGA confirmed the growth of alumina phases (Fig. S10, ESI†). The Al oxidation process was initiated by available oxygen from PVP degradation and then ensued by surrounding air because of ineffective protection by used purge gas (argon and nitrogen) at high TGA furnace temperature. This was evident from the fact that the second stage of oxidation was accelerated when nitrogen was the purge gas (Fig. S11, ESI†), while it was rapid in the oxygen atmosphere. A similar oxidation of Al in the Ar/N_2 environment was reported previously.[23] This explained the protection of embedded Al nanoparticles by PVP from any significant oxidation below degradation, but after PVP removal the oxidation of exposed Al nanoparticles was ensued in the heating environment of the TG-DTA instrument. Progressive air oxidation of polymer coated Al nanoparticles was monitored by PXRD with frequent time intervals over one year and found to be stable (Fig. S12, ESI†). It is worth mentioning that Heting Li *et al.* have reported a template assisted synthesis of Al nanoparticles in an ionomer membrane.[24]

4. Conclusions

The isolation of Al nanoparticles by the reaction described here clearly established the products formed in the reaction of $SiCl_4$ with $LiAlH_4$ and clarified the doubts in the previous reports.[5,6,8] The formation of Al nanoparticles by this reaction was confirmed using various tools like PXRD patterns, TEM images and ^{27}Al MAS-NMR spectra. The sonochemical procedure described here was utilized to produce spherical aluminium nanoparticles having fairly narrow (2–15 nm) size distribution, which were embedded at random locations of the PVP matrix. Thermal analysis of the composites revealed their stability up to 422 °C by progressive oxidation in air.

Acknowledgements

The authors thank the Centre for Nanotechnology at the University of Hyderabad for the TEM facility. Both SNG and SKP acknowledge UGC and DRDO-India for doctoral fellowship.

Notes and references

1 Y. S. Cho, S.-H. Kang, J. S. Han, B. R. Yoo and I. N. Jung, *J. Am. Chem. Soc.*, 2001, **123**, 5584–5585.
2 B. H. Han and P. Boudjouk, *Organometallics*, 1983, **2**, 769–771.
3 (*a*) K. Kim, D. Woo, J. S. Doo and T. Kim, *J. Korean Phys. Soc.*, 2009, **54**, 1021–1026; (*b*) R. M. Sankaran, D. Holunga,

R. C. Flagan and K. P. Giapis, *Nano Lett.*, 2005, **5**, 537–541; (*c*) R. K. Baldwin, K. A. Pettigrew, E. Ratai, M. P. Augustine and S. M. Kauzlarich, *Chem. Commun.*, 2002, 1822–1823.

4 (*a*) G. W. Fester, J. Wagler, E. Brendler, U. Böhme, D. Gerlach and E. Kroke, *J. Am. Chem. Soc.*, 2009, **131**, 6855–6864; (*b*) G. W. Fester, J. Eckstein, D. Gerlach, J. Wagler, E. Brendler and E. Kroke, *Inorg. Chem.*, 2010, **49**, 2667–2673; (*c*) G. W. Fester, J. Wagler, E. Brendler and E. Kroke, *Eur. J. Inorg. Chem.*, 2008, 5020–5023.

5 (*a*) J. Veinot, E. Fok, K. Boates and J. MacDonald, *Chem. Eng. News*, 2005, **83**, 1–4; (*b*) A. S. Wells, *Org. Process Res. Dev.*, 2010, **14**, 484.

6 (*a*) A. E. Finholt, A. C. Bond. Jr and H. I. Schlesinger, *J. Am. Chem. Soc.*, 1947, **69**, 1199–1203; (*b*) A. E. Finholt, A. C. Bond. Jr., K. E. Wilzbach and H. I. Schlesinger, *J. Am. Chem. Soc.*, 1947, **69**, 2692–2696; (*c*) G. D. Barbaras, C. Dillard, A. E. Finholt, T. Wartik, K. E. Wilzbach and H. I. Schlesinger, *J. Am. Chem. Soc.*, 1951, **73**(10), 4585–4590.

7 (*a*) P. K. Sudeep, Z. Page and T. Emrick, *Chem. Commun.*, 2008, 6126–6127; (*b*) X. Cheng, R. Gondosiswanto, S. Ciampi, P. J. Reece and J. J. Gooding, *Chem. Commun.*, 2012, **48**, 11874–11876; (*c*) J. Wang, S. Sun, F. Peng, L. Cao and L. Sun, *Chem. Commun.*, 2011, **47**, 4941–4943; (*d*) J. H. Warner, A. Hoshino, K. Yamamoto and R. D. Tilley, *Angew. Chem., Int. Ed.*, 2005, **44**(29), 4550–4554; (*e*) M. Rosso-Vasic, E. Spruijt, Z. Popović, K. Overgaag, B. V. Lagen, B. Grandidier, D. Vanmaekelbergh, D. Domínguez-Gutiérrez, L. D. Cola and H. Zuilhof, *J. Mater. Chem.*, 2009, **19**, 5926–5933.

8 J. A. Haber and W. E. Buhro, *J. Am. Chem. Soc.*, 1998, **120**, 10847–10855.

9 (*a*) S. R. Ghanta and K. Muralidharan, *J. Nanopart. Res.*, 2013, **15**, 1715–1725; (*b*) S. R. Ghanta and K. Muralidharan, *Nanoscale*, 2010, **2**, 976–980.

10 S. R. Ghanta, M. H. Rao and K. Muralidharan, *Dalton Trans.*, 2013, **42**, 8420–8425.

11 (*a*) B. G. Kumar and K. Muralidharan, *Eur. J. Inorg. Chem.*, 2013, 2102–2108; (*b*) B. G. Kumar and K. Muralidharan, *J. Mater. Chem.*, 2011, **30**, 11271–11275.

12 R. F. Nystrom and W. G. Brown, *J. Am. Chem. Soc.*, 1948, **70**(11), 3738–3740.

13 F. M. Brower, N. E. Matzek, P. F. Reigler, H. W. Rinn, C. B. Roberts, D. L. Schmidt, J. A. Snover and K. Terada, *J. Am. Chem. Soc.*, 1976, **98**(9), 2450–2453.

14 (*a*) J. A. Jegier and W. L. Gladfelter, *Coord. Chem. Rev.*, 2000, **206–207**, 631–650; (*b*) G. Sandrock, J. Reilly, J. Graetz, W.-M. Zhou, J. Johnson and J. Wegrzyn, *Appl. Phys. A: Mater. Sci. Process.*, 2005, **80**, 687–690; (*c*) S. K. Konovalov and B. M. Bulychev, *Inorg. Chem.*, 1995, **34**, 172–175.

15 A. S. H. Fischer and M. C. Grubelich, *Theoretical energy release of thermites, intermetallics and combustible metals*, International Pyrotechnics Seminar, 1998, pp. 1–59.

16 (*a*) N. Arora and B. R. Jagirdar, *J. Mater. Chem.*, 2012, **22**, 9058–9063; (*b*) R. J. Jouet, A. D. Warren, D. M. Rosenberg, V. J. Bellitto, K. Park and M. R. Zachariah, *Chem. Mater.*, 2005, **17**, 2987–2996; (*c*) S. W. Chung, E. A. Guliants, C. E. Bunker, D. W. Hammerstroem, Y. Deng, M. A. Burgers, P. A. Jelliss and S. W. Buckner, *Langmuir*, 2009, **25**, 8883–8887; (*d*) T. J. Foley, C. E. Johnson and K. T. Higa, *Chem. Mater.*, 2005, **17**, 4086–4091; (*e*) K. A. S. Fernando, M. J. Smith, B. A. Harruff, W. K. Lewis, E. A. Guliants and C. E. Bunker, *J. Phys. Chem. C*, 2009, **113**, 500–503.

17 (*a*) M. B. Pomfret, D. J. Brown, A. Epshteyn, A. P. Purdy and J. C. Owrutsky, *Chem. Mater.*, 2008, **20**, 5945–5947; (*b*) M. E. Smith, *Appl. Magn. Reson.*, 1993, **4**, 1–64.

18 R. Bhattacharya, T. N. Phaniraj and D. Shailaja, *J. Membr. Sci.*, 2003, **227**, 23–27.

19 B. H. Toby, *Powder Diffr.*, 2006, **21**, 67–70.

20 L. Chen, W. Song, J. Lv, X. Chen and C. Xie, *Mater. Chem. Phys.*, 2010, **120**, 670–675.

21 S. Hasani, M. Panjepour and M. Shamanian, *Open Access Scientific Reports*, 2012, **1**, 1–7.

22 (*a*) A. R. J. Helmich and K. S. Suslick, *Chem. Mater.*, 2010, **22**, 4835–4837; (*b*) M. A. Trunov, M. Schoenitz and E. L. Dreizen, *Combust. Theory Modell.*, 2006, **10**, 603–623.

23 (*a*) E. L. Dreizin, *Prog. Energy Combust. Sci.*, 2009, **35**, 141–167; (*b*) M. A. Trunov, S. M. Umbrajkar, M. Schoenitz, J. T. Mang and E. L. Dreizin, *J. Phys. Chem. B*, 2006, **110**, 13094–13099.

24 H. Li, M. J. Meziani, F. Lu, C. E. Bunker, E. A. Guliants and Y. P. Sun, *J. Phys. Chem. C*, 2009, **113**, 20539–20542.